

## Excimer Laser Crystallization of Nanocrystalline Silicon Thin Films

Lijie DENG<sup>a</sup>, Wei HE<sup>b</sup> and Zhengping LI<sup>c\*</sup>

Laboratory of Condensed Matter Spectroscopy and Opto-Electronic Physics, Key Laboratory of Artificial Structures and Quantum Control (Ministry of Education), Institute of Solar Energy, Department of Physics and Astronomy, Shanghai Jiao Tong University, 800 Dong Chuan Road, Shanghai 200240, People's Republic of China

<sup>a</sup>wjtdlj@situ.edu.cn, <sup>b</sup>hewei863@126.com, <sup>c</sup>zpli@situ.edu.cn

**Keywords:** Excimer laser crystallization; nanocrystalline silicon; thin film; Raman spectra; surface roughness

**Abstract.** Nanocrystalline silicon (nc-Si) thin film on glass substrate is subjected to excimer laser crystallized by varying the laser energy density in the range of 50~600 mJ/cm<sup>2</sup>. The effect of excimer laser crystallization on the structure of silicon film is investigated using Raman spectroscopy, X-ray diffraction, atomic force microscopy and scanning electron microscopy. The results show that polycrystalline silicon thin films can be obtained by excimer laser crystallization of nc-Si films. A laser threshold energy density of 200 mJ/cm<sup>2</sup> is estimated from the change of crystalline fraction and surface roughness of the treated films. The growth of grain is observed and the crystallization mechanism is discussed based on the super lateral growth model. The nanocrystalline silicon grains in the films act as seeds for lateral growth to large grains.

### Introduction

The technology of low-temperature polycrystalline silicon (poly-Si) thin film transistors (TFTs) has been widely investigated for application in active matrix flat panel display[1-3]. Various methods for fabricating high-quality poly-Si films with large grain size, low defect density, and high carrier mobility have been reported. These include excimer laser crystallization (ELC)[3-7], solid-phase crystallization (SPC)[4,8], and metal-induced lateral crystallization (MILC)[2,8]. Among these technologies, ELC has been employed as a promising option in industries for preparing poly-Si thin films for TFTs. ELC is a rapid crystallization technique that is characterized by melting of thin films and following solidification within several tens of nanoseconds (ns), often without affecting the underlying substrate. This technique enables the use of inexpensive substrates, such as glass, which are highly preferable for low cost, large-area electronic devices. Although the application has primarily been focused on TFTs, its adaptability for photovoltaics (PV) has also attracted considerable interests[9-11].

The hydrogenated amorphous silicon (a-Si:H) is usually used as starting material for ELC. The ELC of a-Si:H films and the physics of ELC have been investigated extensively[12,13]. A laser threshold energy density exists for the conversion of a-Si:H to polycrystalline silicon, corresponding to the threshold for surface melting[1]. Films start to melt after this energy density, and the melt depth increasing with increase of energy density. Three basic transformation scenarios, partial melting, complete melting, and near complete melting regimes, have been reported which primarily depend on energy density and initial film thickness during ELC[12,13]. Partial melting occurs when the laser energy is low, but sufficient to melt a layer of the film leaving a continuous solid layer underneath. This regime results in a stratified structure with large crystallites at the irradiating surface, followed by a fine-grained silicon layer. In the complete melting regime, the deeply supercooled melt increases nucleation rate causing a spontaneous process. The resulting films have a fine-grained crystalline structure. Between the two major regimes, another regime called "near complete melting regime" exists. It was regarded that, just before the complete melt, the unmelted portion of the underlying silicon consists of islands of solids instead of a continuous layer. These unmelted solids separated by small local regions of completely melted silicon act as seed layers for lateral growth[13]. The lateral growth results in very large grain sizes, a few times that of the film thickness[13].

However, a-Si:H film is with disordered structure, no crystallinity, and no silicon grains in its tissue. In the literature [14], the ELC of microcrystalline silicon ( $\mu\text{c-Si:H}$ ) with grain diameter of 20-30 nm was mentioned, and the stress in films was calculated. Microcrystalline silicon for TFTs on glass and plastics substrates were performed [15-17], the  $\mu\text{c-Si:H}$  was with 25-60 nm grain size, about 70% of crystalline fraction ( $X_c$ ), and 200 nm of thickness. Crystallization of  $\mu\text{c-Si}$  process could be different as crystalline grains are presented in the starting material. Hydrogenated nanocrystalline silicon (nc-Si:H) thin film is a two-phase mixed material constituting of nanostructured crystalline silicon and amorphous silicon. The silicon grains are usually in several nanometer and are embedded in the Si:H amorphous tissues [18,19]. The research on ELC of nc-Si:H films has not been reported in the literatures. The effect of nanocrystalline silicon grains in nc-Si:H on the ELC of silicon thin films is not known. Here, in the present work, nc-Si:H films with a typical silicon grain size of several nanometer deposited on glass substrate were excimer-laser-crystallized by varying excimer laser energy density. The purpose of this work is to investigate the microstructure changes of nc-Si:H after ELC.

Another problem is the thickness of deposited thin films. The ability of excimer laser to crystallize a very thin layer of a-Si:H in the order of 100 nm becomes a limitation for photovoltaics, since films of the order 1  $\mu\text{m}$  are necessary for light absorption [20]. Larger thickness means higher laser fluence needed for the crystallization [21]. It is concluded that it is not possible to convert a-Si:H films thicker than 300 nm completely to polycrystalline silicon without utilizing laser energy densities in excess of 200  $\text{mJ/cm}^2$  [22]. The target of the work is to attempt the feasibility of nc-Si:H which is recrystallized by ELC in photovoltaics application. Consequently, the nc-Si:H films with about 1  $\mu\text{m}$  thick, which is adequately thick for light absorption for photovoltaics application, are deposited and then subjected to ELC.

## Experiment

The nc-Si:H thin films were prepared from highly hydrogen ( $\text{H}_2$ ) diluted silane ( $\text{SiH}_4$ ) in a 13.56 MHz parallel plate plasma enhanced chemical vapor deposition (PECVD) system. The substrate chosen for the experimental study was inexpensive Corning 1737 glass and the substrate temperature was 250  $^\circ\text{C}$ . The as-deposited nc-Si:H films were placed in a  $5 \times 10^{-4}$  Pa vacuum chamber and were irradiated by an XeCl excimer laser (beam size around 1 cm  $\times$  1 cm) operating at 308 nm with 20 ns full-width at half-maximum (FWHM) pulse duration at room temperature through a quartz window. The laser energy density was varied from 50 to 600  $\text{mJ/cm}^2$ . Due to the pulse-to-pulse variation of excimer laser energy, it is estimated that the measured energy densities have an error up to 10% [23]. The Raman spectra were performed on a Jobin Yvon LabRam HR800UV micro-Raman spectrometer to estimate the  $X_c$  of the samples. The X-ray diffraction (XRD) patterns of the resultant films were measured on a Bruker D-8 XRD system with a Cu  $K\alpha$  radiation (40 kV, 60 mA). The laser crystallized silicon surfaces were investigated by using atomic force microscopy (AFM) on a BIOSCOPE<sup>TM</sup> instrument. The microstructural analyses of samples were performed by field emission scanning electron microscopy (FE-SEM) on a FEI Nova NanoSEM 230 system.

## Results and Discussion

For the structural investigation of the nc-Si:H thin films treated with increasing laser energy density, we carried out micro-Raman and XRD measurements. The evolution of Raman spectra of samples treated with increasing laser energy density are presented in Fig. 1. In Fig. 1(a), the experimental Raman spectrum can be decomposed into four Gaussian phonon bands (dashed curves) by the strain-incorporated three-dimensional phonon confinement model, among which three peaks from the a-Si phase (longitudinal acoustic (LA) band centered at 300  $\text{cm}^{-1}$ , the longitudinal optical (LO) band at 380  $\text{cm}^{-1}$ , and the transverse optical (TO1) band at 480  $\text{cm}^{-1}$ ) and one from the c-Si phase (asymmetric transverse optical (TO2) band at around 520  $\text{cm}^{-1}$ ). In Fig. 1(b),

we show spectrum of the sample treated with laser energy density of  $200 \text{ mJ/cm}^2$ . It can be found that there is no much difference with that of the nc-Si:H thin film. But the sample treated with laser energy density of  $300 \text{ mJ/cm}^2$  clearly has higher  $X_c$ , which can be seen from Fig. 1(c). In Fig. 1(d), the treated laser energy density is  $600 \text{ mJ/cm}^2$ ,  $X_c$  of the sample is approximately 100% because no transverse-optical phonon is found in the spectrum[6].

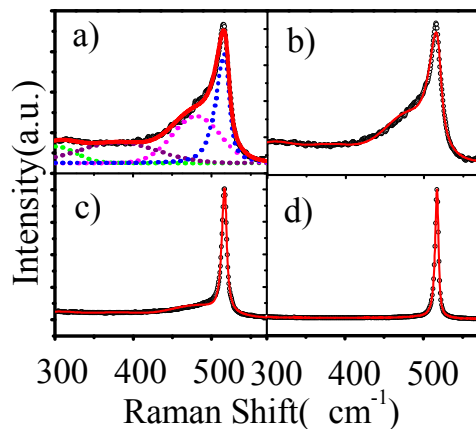


Fig. 1. Raman spectra of as-deposited nc-Si thin film and the resulting films EL crystallized at different laser energy densities. (a) nc-Si film (b)  $200 \text{ mJ/cm}^2$ , (c)  $300 \text{ mJ/cm}^2$ , and (d)  $600 \text{ mJ/cm}^2$ .

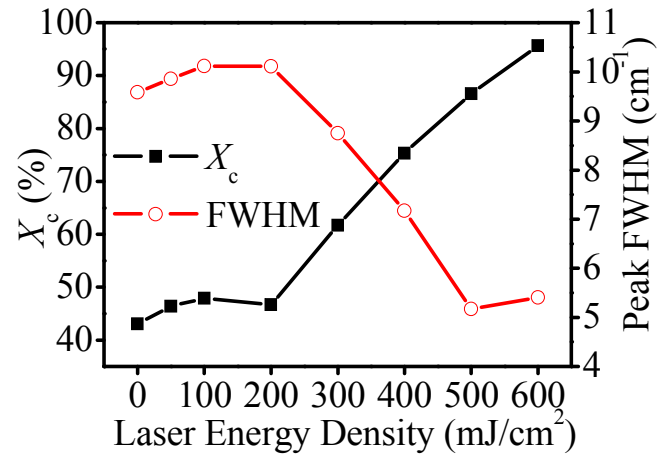


Fig. 2. Crystalline fraction  $X_c$  deduced from Raman spectra and FWHM of crystalline TO band as a function of laser energy density.

In Fig. 2 we show  $X_c$  of the samples varying with laser energy density and the FWHM of the the Raman spectra for crystalline TO phonon band in detail. The  $X_c$  of samples is determined by using  $X_c = I_c / (I_c + \eta I_a)$ , where  $I_c$  and  $I_a$  are the integrated intensities of  $\text{TO}_2$  and  $\text{TO}_1$  Raman modes, respectively,  $\eta$  is the ratio of the backscattering cross-sections amorphous and crystalline phases. The selection of a value for  $\eta$  is complex due to its dependency on absorption coefficient of amorphous and crystalline silicon. Here,  $\eta$  was taken to be 0.8[22]. It is observed that the  $X_c$  remains in the level of 43-48% but a bit increasing before  $200 \text{ mJ/cm}^2$ , and an obvious trend of increasing  $X_c$  with increasing of laser energy density from  $200$  to  $600 \text{ mJ/cm}^2$ . Similarly, for laser energy below  $200 \text{ mJ/cm}^2$ , FWHM is relatively large, being attributed to the effect of microcrystals grains smaller than a few ten nm[4]. For the larger laser energy density region, FWHM is regarded to be dominated by defect density because grain size is sufficiently large to neglect the microcrystal effect[4]. When the laser energy density is  $600 \text{ mJ/cm}^2$ , the FWHM of Raman spectrum of approximately  $5.4 \text{ cm}^{-1}$  is clearly observed, which indicates that the films are sufficiently crystallized[6].

The re-crystallization process of nc-Si:H seems similar to those of amorphous silicon. It shows a threshold estimated from which the shape of Raman spectra change distinctly, the  $X_c$  increases and the FWHM decreases. The threshold of laser energy density is estimated to be  $200 \text{ mJ/cm}^2$  from the change of  $X_c$  in the present work.

Fig. 3 shows the XRD patterns of samples crystallized with different laser energy densities. The as-deposited nc-Si:H film only show a weak and broad (111) diffraction peak. A clear trend of increasing crystallinity is observed as expected from ELC. After  $50 \text{ mJ/cm}^2$  EL crystallized, the (111) diffraction peak becomes more visible, and the (220) diffraction peak emerges. The situations for  $100$  and  $200 \text{ mJ/cm}^2$  are the same. When the energy density reaches to  $300 \text{ mJ/cm}^2$ , the (111) and (220) diffraction peaks become prominent comparing with that of lower energy densities. This indicates that the crystallinity is much larger than that of lower energy densities. Furthermore, the

(111) and (220) diffraction peaks become very sharp when the laser energy densities reach to 500 and 600  $\text{mJ}/\text{cm}^2$ , indicating that the crystallinity of these two samples is close to crystalline silicon.

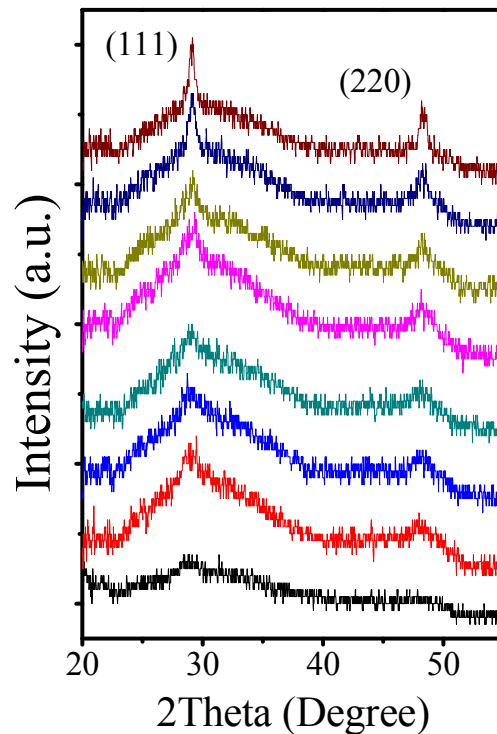


Fig. 3. XRD patterns of samples EL crystallized at an increasing energy density, from bottom to up corresponding to nc-Si, 50, 100, 200, 300, 400, 500, and 600  $\text{mJ}/\text{cm}^2$ .

In the region of laser energy density from 50 to 200  $\text{mJ}/\text{cm}^2$ , the XRD patterns show that the crystallinity increase comparing with that of as-deposited nc-Si:H film. But the Raman results do not indicate the increase of crystallinity when the energy density in the range of 50 to 200  $\text{mJ}/\text{cm}^2$ , because the change in Raman spectra with increasing laser density is slow[16]. After a threshold of 200  $\text{mJ}/\text{cm}^2$ , the increase of crystallinity because of ELC become prominent, evidenced by the sharpening of (111) and (222) diffraction peaks.

The AFM observations of the surface of samples crystallized at increasing laser energy are shown in Fig. 4. The dense structure of islands is visible on the surface of the as-deposited film. With the increase of laser energy density, we observe smoothing out of the surface according to the surface morphology changes in samples treated with 50 and 100  $\text{mJ}/\text{cm}^2$ . This is the results of self-organization[24] of nc-Si introduced by laser beam. The samples show gradual grain growth with increasing laser energy density from 200 to 600  $\text{mJ}/\text{cm}^2$ . Grain size reaches nearly 700 nm for 600  $\text{mJ}/\text{cm}^2$ . When the laser energy is high, the grain looks like a pyramid structure which always shows in monocrystalline silicon textured with alkali solution. The pyramid-like structure is highly desirable for light trapping in photovoltaic applications. This quality of EL crystallized silicon can be very advantageous if the process is tailored for solar cell application, yielding a surface texturing without additional cost[22].

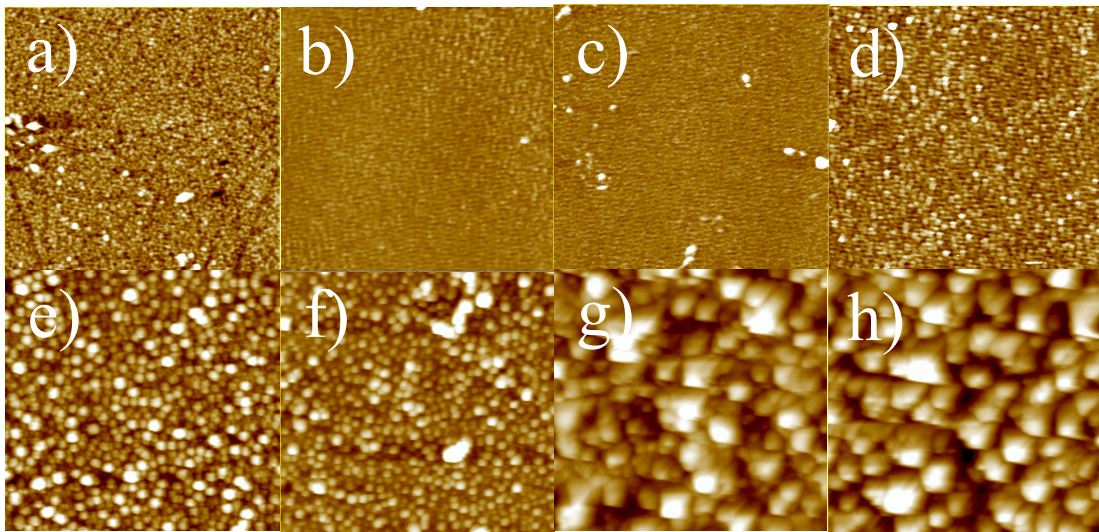


Fig. 4. AFM observation of the surface ( $10 \mu\text{m} \times 10 \mu\text{m}$ ) of different samples crystallize at various laser energy densities, (a) nc-Si film, (b)  $50 \text{ mJ/cm}^2$ , (c)  $100 \text{ mJ/cm}^2$ , (d)  $200 \text{ mJ/cm}^2$ , (e)  $300 \text{ mJ/cm}^2$ , (f)  $400 \text{ mJ/cm}^2$ , (g)  $500 \text{ mJ/cm}^2$ , and (h)  $600 \text{ mJ/cm}^2$ .

Surface roughnesses of the films are estimated by AFM over a  $100 \mu\text{m}^2$  area. Fig. 5 shows RMS roughness variation with laser energy density. A RMS threshold is evidenced at  $200 \text{ mJ/cm}^2$ . Before

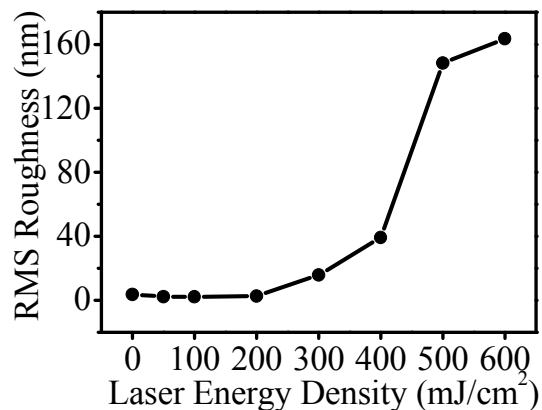


Fig. 5. RMS roughness of resulting silicon films versus laser energy density showing a threshold at  $200 \text{ mJ/cm}^2$ .

this threshold, the laser energy is not enough to melt a part of the film and then to change the as-deposited nanocrystalline structure. Therefore, RMS roughness is nearly constant. At this threshold, a sudden increase of roughness starts. Explosive evaporating of hydrogen is expected to be the principle reason for surface roughness to occur[25]. The behavior is different from what was observed for excimer laser crystallization of amorphous silicon. In the case of a-Si, the surface roughness gradually increases as the laser energy density increases. The difference is ascribed to the different absorption coefficient of a-Si and crystalline silicon [16], a-Si begins to crystallize at low laser energy whereas higher energy is needed to alter the crystalline structure of crystalline silicon[16]. In the present work, the crystalline silicon is nc-Si.

Fig. 6 shows the SEM pictures of the film crystallized at various laser energy densities. As can be seen, the surface microstructures of the films irradiated at 50 and  $100 \text{ mJ/cm}^2$  become smoothing comparing with that of as-deposited film. It is clearly showed that the average grain size increases from tens of nm to hundreds of nm with the increase in excimer laser energy density from 200 to  $600 \text{ mJ/cm}^2$ .

The crystallization mechanism can be explained following the super lateral growth (SLG) model[12,13], especially the “controlled SLG (C-SLG)”[23,26]. In the present case, the

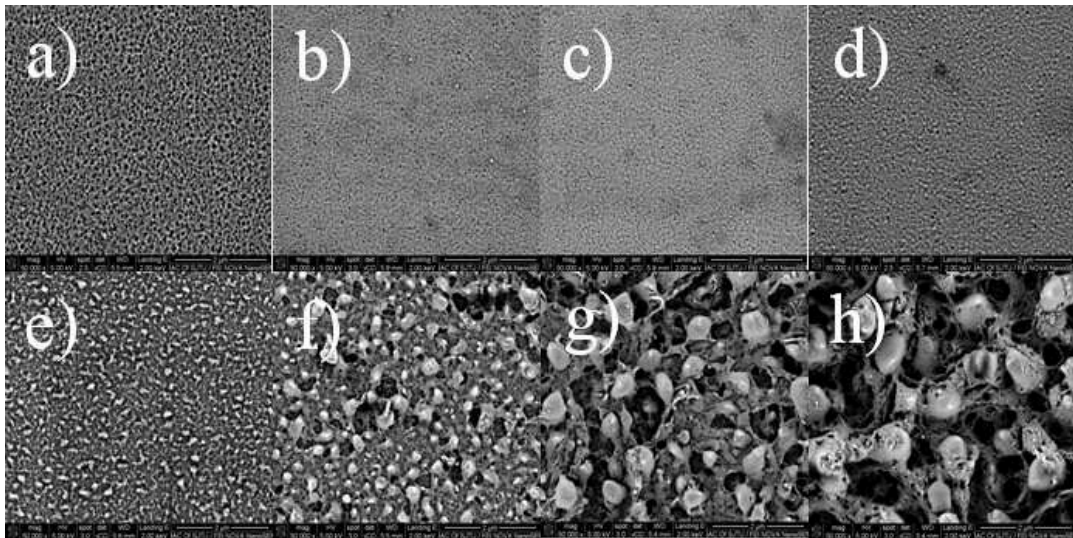


Fig. 6. SEM morphology ( $2\ \mu\text{m} \times 2\ \mu\text{m}$ ) of films irradiated at various laser energy densities, (a) nc-Si film, (b)  $50\ \text{mJ}/\text{cm}^2$ , (c)  $100\ \text{mJ}/\text{cm}^2$ , (d)  $200\ \text{mJ}/\text{cm}^2$ , (e)  $300\ \text{mJ}/\text{cm}^2$ , (f)  $400\ \text{mJ}/\text{cm}^2$ , (g)  $500\ \text{mJ}/\text{cm}^2$ , and (h)  $600\ \text{mJ}/\text{cm}^2$ .

as-deposited film contains nanocrystalline silicon and crystalline fractions. Initially, the film will not melt completely as the crystalline fractions have a higher melting temperature than the amorphous matrix in which they are embedded. At low energy, only an up part of the film is melted and crystallization starts from the grains of unmelted bottom part. When the fluence increases, the deep part of the nanocrystalline film is melted. It shows a threshold from the plot of surface roughness versus laser energy. The threshold value represents the energy density for which the nanocrystalline silicon grains reach the melting point. The increase of RMS roughness correlates with increasing grain size[16]. Lateral growth is more important, that leads to large grains. SLG occurs as a consequence of the lowering in the free energy of the solid-Si/molten-Si system, by the growth of the former (solid-Si) into the undercooled liquid (molten-Si) region[23]. When the laser energy density is more than  $200\ \text{mJ}/\text{cm}^2$ , it is sufficient to completely melt the amorphous part of the films, while the nanocrystalline silicon grains in the films act as seeds for lateral growth of material into the undercooled liquid. The nanocrystalline silicon grains are not melted completely though the laser fluence has reached  $600\ \text{mJ}/\text{cm}^2$ . The process window of SLG is widened because of the existence of nanocrystalline silicon grains in the films, i.e. the ELC of nc-Si:H films in the present case is followed the SLG in a wide range of laser energy density.

ELC of a-Si usually shows the decreasing of grain size and crystalline fraction beyond a laser energy threshold corresponding to the full melting of film layer, the energy for complete melting of nc-Si should be high. However, even if the full melt threshold (FMT) is not reached, the obtained crystalline fraction (Fig. 2) is sufficiently high and much higher than its initial value.

## Conclusions

The nc-Si:H thin film on glass substrate is crystallized by excimer laser with a laser energy density of  $50\text{-}600\ \text{mJ}/\text{cm}^2$ . The crystallized thin films have been characterized by Raman spectra, XRD, AFM and SEM. Poly-Si films with higher crystallinity can be obtained by ELC method. A threshold value of  $200\ \text{mJ}/\text{cm}^2$  is estimated from plots of crystalline fraction and RMS surface roughness versus laser energy density. The amorphous part in the nc-Si:H film is partially melted before the threshold. While the nc-Si grains begin to melt after energy density passed threshold. The nc-Si grains in the films serve as seeds for lateral growth to large grains during the process of ELC. The existence of nc-Si grains in the films widens the process window of SLG.

## Acknowledgements

This work was supported by the National High Technology R&D Project of China (2011AA050502).

## References

- [1] S.D. Brotherton, D.J. McCulloch, J.P. Gowers, J.R. Ayres, M.J. Trainor, Influence of melt depth in laser crystallized poly-Si thin film transistors, *J. Appl. Phys.* 82 (1997) 4086-4094.
- [2] P.I. Widenborg, A.G. Aberle, Hydrogen-induced dopant neutralisation in p-type AIC poly-Si seed layers functioning as buried emitters in ALICE thin film solar cells on glass, *J. Cryst. Growth* 306 (2007) 177-186.
- [3] A. Baiano, R. Ishihara, J. Van der Cingel, K. Beenakker, Strained single-grain silicon n- and p-channel thin-film transistors by excimer laser, *IEEE Electr. Device Lett.* 31 (2010) 308-310.
- [4] K. Kitahara, K. Ohnishi, Y. Katoh, R. Yamazaki, T. Kurosawa, Analysis of defects in polycrystalline silicon thin films using Raman scattering spectroscopy, *Jpn. J. Appl. Phys.* 42 (2003) 6742-6747.
- [5] J. Viatella, R.K. Singh, Transient recrystallization of amorphous silicon films, *Mat. Sci. Eng. B-Solid* 47 (1997) 78-86.
- [6] C.-C. Kuo, Micro-Raman spectroscopy characterization of polycrystalline silicon films fabricated by excimer laser crystallization, *Opt. Laser. Eng.* 47 (2009) 612-616.
- [7] A.A.D.T. Adikaari, N.K. Mudugamuwa, S.R.P. Silva, Use of an asymmetric pulse profile for higher crystalline volumes from excimer laser crystallization of amorphous silicon, *Appl. Phys. Lett.* 90 (2007) 171912.
- [8] S. Gall, C. Becker, K.Y. Lee, T. Sontheimer, B. Rech, Growth of polycrystalline silicon on glass for thin-film solar cells, *J. Cryst. Growth* 312 (2010) 1277-1281.
- [9] A.A.D.T. Adikaari, N.K. Mudugamuwa, S.R.P. Silva, Nanocrystalline silicon solar cells from excimer laser crystallization of amorphous silicon, *Sol. Energy Mater. Sol. Cells* 92 (2008) 634-638.
- [10] N.K. Mudugamuwa, A.A.D.T. Adikaari, D.M.N.M. Dissanayake, V. Stolojan, S.R.P. Silva, Reversible increase of photocurrents in excimer laser-crystallized silicon solar cells, *Sol. Energy Mater. Sol. Cells* 92 (2008) 1378-1381.
- [11] W.-C. Yeh, M. Matsumura, Preparation of giant-grain seed layer for poly-silicon thin-film solar cells, *Jpn. J. Appl. Phys.* 38 (1999) L110-L112.
- [12] J.S. Im, H.J. Kim, M.O. Thompson, Phase transformation mechanisms involved in excimer laser crystallization of amorphous silicon films, *Appl. Phys. Lett.* 63 (1993) 1969-1971.
- [13] J.S. Im, H.J. Kim, On the super lateral growth phenomenon observed in excimer laser-induced crystallization of thin Si films, *Appl. Phys. Lett.* 64 (1994) 2303-2305.
- [14] S. Higashi, N. Ando, K. Kamisako, T. Sameshima, Stress in pulsed-laser-crystallized silicon films, *Jpn. J. Appl. Phys.* 40 (2001) 731-735.
- [15] T. Pier, K. Kandoussi, C. Simon, N. Coulon, H. Lhermite, T. Mohammed-Brahim, J.F. Bergamini, Microcrystalline silicon and excimer laser crystallized silicon thin film transistors on the same substrate, *Thin Solid Films* 515 (2007) 7585-7589.
- [16] T. Pier, K. Kandoussi, C. Simon, N. Coulon, T. Mohammed-Brahim, H. Lhermite, Excimer laser crystallization of microcrystalline silicon for TFTs on flexible substrate, *J. Non-cryst. Solids* 354 (2008) 2300-2304.

- [17] T. Pier, K. Kandoussi, C. Simon, N. Coulon, T. Mohammed-Brahim, H. Lhermite, Excimer laser annealing of microcrystalline silicon, *Phys. Stat. Sol. C* 5 (2008) 3234-3238.
- [18] Y.L. He, C.Z. Yin, G.X. Cheng, L.C. Wang, X.N. Liu, G.Y. Hu, The structure and properties of nanosize crystalline silicon films, *J. Appl. Phys.* 75 (1994) 797-803.
- [19] K.H. Li, W.Z. Shen, Uniformity and bandgap engineering in hydrogenated nanocrystalline silicon thin films by phosphorus doping for solar cell application, *J. Appl. Phys.* 106 (2009) 063505.
- [20] H. Keppner, J. Meier, P. Torres, D. Fischer, A. Shah, Microcrystalline silicon and micromorph tandem solar cells, *Appl. Phys. A-Mater.* 69 (1999) 169-177.
- [21] M.R. Semler, J.M. Hoey, S. Guruvenket, C.R. Gette, O.F. Swenson, E.K. Hobbie, Structural and electronic characterization of 355 nm laser-crystallized silicon: Interplay of film thickness and laser fluence, *J. Appl. Phys.* 115 (2014) 163503.
- [22] A.A.D.T. Adikaari, S.R.P. Silva, Thickness dependence of properties of excimer laser crystallized nano-polycrystalline silicon, *J. Appl. Phys.* 97 (2005) 114305.
- [23] A.T. Voutsas, A new era of crystallization: advances in polysilicon crystallization and crystal engineering, *Appl. Surf. Sci.* 208-209 (2003) 250-262.
- [24] D. Klinger, E. Łusakowska, D. Żymierska, Nano-structure formed by nanosecond laser annealing on amorphous Si surface, *Mat. Sci. Semicon. Proc.* 9 (2006) 323-326.
- [25] D.J. McCulloch, S.D. Brotherton, Surface roughness effects in laser crystallized polycrystalline silicon, *Appl. Phys. Lett.* 66 (1995) 2060-2062.
- [26] J.S. Im, M.A. Crowder, R.S. Sposili, J.P. Leonard, H.J. Kim, J.H. Yoon, V.V. Gupta, H.J. Song, H.S. Cho, Controlled super-lateral growth of Si films for microstructural manipulation and optimization, *Phys. Stat. Sol. A* 166 (1998) 603-617.